Fluid Phase Equilibria 362 (2014) 125–135

Contents lists available at ScienceDirect

Fluid Phase Equilibria

journal homepage: www.elsevier.com/locate/fluid

High pressure phase behavior modeling of asymmetric alkane + alkane binary systems with the RKPR EOS

M. Cismondi Duarte[a,b,*], M.V. Galdo[b], M.J. Gomez[b], N.G. Tassin[b], M. Yanes[b]

[a] IDTQ-PLAPIQUI (Universidad Nacional de Córdoba, CONICET), Argentina
[b] Phasety, Incubadora de Empresas UNC, Córdoba, Argentina

ARTICLE INFO

Article history:
Received 16 July 2013
Received in revised form
15 September 2013
Accepted 18 September 2013
Available online 26 September 2013

Keywords:
Methane
Ethane
Hydrocarbons
High pressure phase behavior
RKPR

ABSTRACT

Very asymmetric hydrocarbon mixtures present an interesting academic challenge for their modeling. In addition, they are becoming more important technologically, since the world oil reserves are becoming heavier in average.

The RKPR EOS was developed in recent years in order to consider asymmetric systems and allow for a good representation of densities for different types of compounds while maintaining the relative simplicity of cubic equations of state. In this work the RKPR EOS is applied for the first time for the correlation of phase behavior in the series of binary systems methane + *n*-alkane and ethane + *n*-alkane. In addition to the use of attractive and repulsive interaction parameters with quadratic mixing rules, the role of the extra degree of freedom that the RKPR model offers for setting the pure compound parameters was also examined. A new table of RKPR pure compound parameters was defined for *n*-alkanes. A comparative study was made with the Peng–Robinson EOS, based on following the same optimization procedure for interaction parameters.

1. Introduction

It is usually assumed that the phase behavior of mixtures composed of different alkanes can be reasonably predicted with classic cubic equations of state (EOS) like SRK or Peng–Robinson (PR) and null interaction parameters (see for example Chapter 5 in Pedersen and Christensen [1]). This can be true in mixtures where the asymmetry in size is not so high. In particular, in binary mixtures of methane or ethane with higher alkanes, acceptable predictions could be obtained up to C_{10}, or C_{16} respectively, at most. But, as it can be seen from Fig. 1 through the comparison of predicted and experimental critical lines, the extension of the high pressure liquid–vapor separation is clearly underestimated for more asymmetric systems, especially for the methane-series and in the range of temperatures around 300 or 400 K, which is of high technological importance for the oil and gas industry.

The RKPR EOS was developed in recent years in order to consider asymmetric systems and allow for a good representation of densities for different types of compounds while maintaining the relative simplicity of cubic equations of state [2]. It has been successfully applied to different types of mixtures and situations and by different research groups in the world [3–7]. The aim in this work is to study the possibilities that the RKPR EOS offers and to exploit its flexibility in order to get the best possible representation of phase behavior for mixtures containing methane and higher *n*-alkanes. The PR EOS, which in preliminary studies showed a better performance than the SRK EOS for these mixtures, will also be implemented for comparison.

2. Experimental data and evolution of fluid phase behavior in the methane and ethane series

We performed a comprehensive review, finding around 70 and 40 articles with published data on fluid phase equilibrium for binary mixtures composed of methane and ethane, respectively, plus a higher alkane. In the first group, i.e., the methane-series, compositional information for both phases in biphasic conditions is common in the systems with alkanes with carbon numbers up to 10. In turn, most of the data for more asymmetric systems consist of isoplethic sets of points obtained through synthetic methods. In particular, a collection of experimental data on the fluid phase behavior of these asymmetric systems, very important in quantity and quality, was contributed from the Technical University of Delft (TU Delft) during the last three decades [8–14]. The binary mixtures of methane with higher *n*-alkanes exhibit phase behavior of type V from C_6 on, and probably of type III for higher carbon numbers like 20 and 30, although the solidification of the paraffin prevents from

* Corresponding author at: IDTQ-PLAPIQUI (Universidad Nacional de Córdoba, CONICET), Argentina. Tel.: +54 351 5353756x16480.
E-mail addresses: cismondi@phasety.com, mcismondi@efn.uncor.edu (M. Cismondi Duarte).

0378-3812/$ – see front matter © 2013 Elsevier B.V. All rights reserved.
http://dx.doi.org/10.1016/j.fluid.2013.09.039

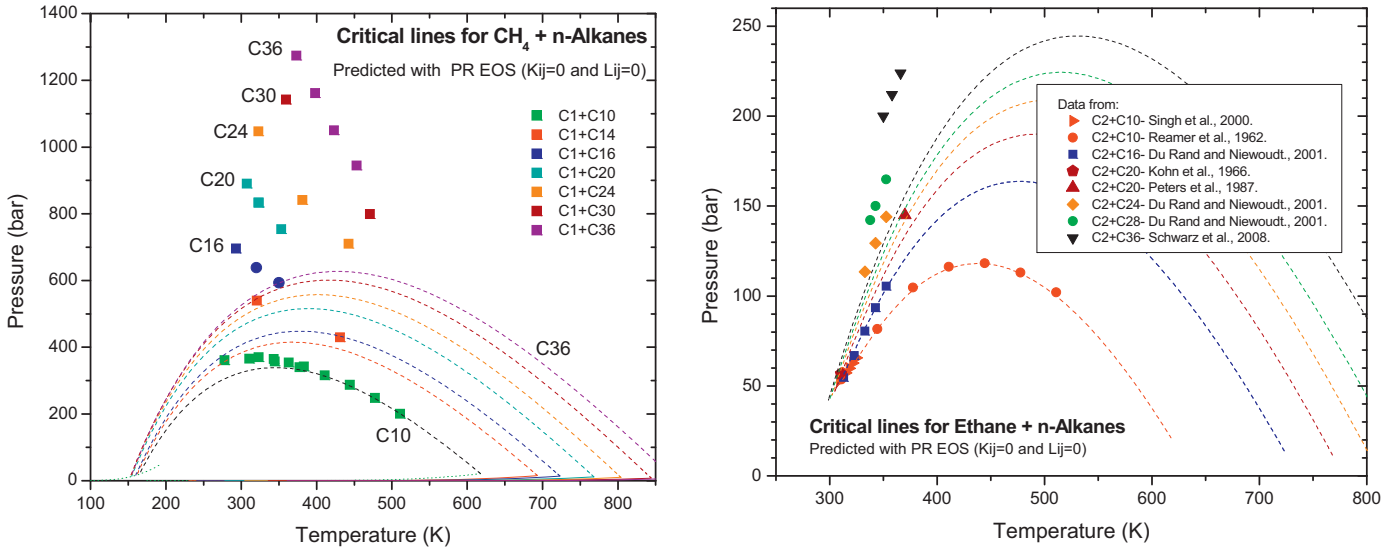

Fig. 1. Prediction of critical lines for methane + *n*-alkane and ethane + *n*-alkane binary systems, with the Peng–Robinson EOS and quadratic mixing rules with null interactions. References for the experimental critical or pseudo-critical points are given in Table A1.

experimentally studying the complete critical lines. Flöter et al. [15] presented a review on the evolution of phase behavior in this series, including coordinates for the second critical end-points of different systems.

With respect to the ethane-series, although not as large as for the methane series, this collection of data is also important, including a considerable diversity of molecular weights and also types of data, from analytic methods (compositional information for both phases in biphasic conditions) to synthetic methods informing either vapor or dew pressures, both far from and close to the critical region depending on the case, and also LLV data. In particular, a collection of experimental data on the fluid phase behavior of these asymmetric systems, very important in quantity and quality, were contributed by Peters et al., from the Technical University of Delft (TU Delft) between 1986 and 1991 [16–22]. The binary mixtures of ethane with higher *n*-alkanes exhibit phase behavior of type V from C_{18} on, which implies partial miscibility in the liquid phase. Although three-phase liquid–liquid–vapor equilibrium has been experimentally observed and measured up to C_{25}, it is completely obscured by solidification in the mixtures of ethane with C_{26} and higher alkanes [20].

3. Modeling approach and parameterization strategy

In a preliminary study on the correlation of fluid phase equilibria for asymmetric alkane–alkane binary mixtures we found that better results can be achieved with the PR EOS in comparison to SRK, still with important limitations in the most asymmetric cases. We also found that, with the RKPR EOS and pure compound parameters reproducing the saturated liquid density at a reduced temperature of 0.70 [6], the results were comparable to those with PR, a little better or worse, depending on the case.

During the same study we also tried different pure compound parameters for the alkanes by setting free the extra flexibility of the RKPR model, instead of imposing the reproduction of a certain density value for each pure compound. We observed that the performance of the RKPR EOS, in terms of the minimum value that could be achieved for a given objective function, was quite sensitive to the pure compound parameter sets. Therefore, a decision had to be made regarding which pure compound parameters table to use for this work, in addition to the implementation of a mixing rule and the definition of an objective function.

3.1. Pure compound parameters

Besides allowing for the exact reproduction of the experimental T_c and P_c for each fluid, the RKPR EOS provides one extra degree of freedom in comparison to classic two-parameter cubic EOS like SRK or PR, and different approaches were followed in previous articles. In the original RKPR development, Cismondi and Mollerup [2] proposed the relation $Z_c^{EOS} = 1.168\ Z_c^{exp}$ as the default setting for non-associating fluids, which was later followed by other authors [3,4,7]. In other works, Cismondi et al. decided to impose the reproduction of the liquid density at a specified temperature, either at the triple point [5] or at $T_r = 0.70$ [6].

For this work, and in view of our preliminary studies showing that this "pure compound degree of freedom" may have an important effect on the correlation capacity of the model for these type of asymmetric systems, we decided not to impose any general rule or the reproduction of a specific density point. Instead, we followed this strategy: we selected some representative *n*-alkanes, especially C_{10}, C_{16}, C_{20}, C_{24}, C_{36}, and tried different sets of pure compound parameters for each of them, each set defined by a specified value for the third parameter δ_1. We performed multiple minimizations of a given objective function for each system (see Section 3.3), in order to see which set of parameters led to the lowest value of the minimized function for each system. Paying attention to both series of binary systems, and adjusting to a regular soft trend, we finally came to the parameter sets presented in Table 1 for all the alkanes considered in this work. In order to have a reference to compare with the original rule proposed in the original RKPR paper [2], the implied Z_c ratio is also included in the table. It can be seen that the value of 1.168 was only slightly modified for methane, but the departure increases with the chain length of the alkane.

The third parameter can be interpreted as a structural parameter, which increases with non-sphericity (and also with polarity, but polarity is not present in alkanes). Then, one would expect δ_1 to increase continuously with carbon number. In turn, Table 1 presents a maximum value of 2.55 for C_{20}, then decreasing to 1.70 for C_{36}, the longest alkane considered. This trend, in principle surprising, may appear as the natural one if we consider that a sort of *effective* non-sphericity of the molecule, in average, should reach a maximum at some point and then decrease, due to the molecular folding that takes place, based on the rotation of the chain bonds.

Table 1
Pure compound parameters for the RK-PR EOS (this work).

Compound	ID	Z_c^{EOS}/Z_c^{exp}	a_c (bar L^2/mol^2)	b (L/mol)	δ_1	K	T_c	P_c	ω
Methane	C_1	1.1717	2.3213	0.030088	0.85	1.50758	190.564	45.99	0.01155
Ethane	C_2	1.1883	5.6766	0.044874	1.10	1.85920	305.320	48.72	0.09949
Propane	C_3	1.1921	9.6133	0.061731	1.25	2.04972	369.830	42.48	0.15229
n-Butane	C_4	1.1932	14.3122	0.078573	1.40	2.21155	425.120	37.96	0.20016
n-Pentane	C_5	1.2031	19.7728	0.097066	1.50	2.39339	469.700	33.70	0.25151
n-Hexane	C_6	1.2151	25.8505	0.115976	1.60	2.56306	507.600	30.25	0.30126
n-Decane	C_{10}	1.2797	55.9827	0.195979	2.00	3.17836	617.700	21.10	0.49233
n-Tetradecane	C_{14}	1.3630	96.4756	0.286570	2.37	3.59412	693.000	15.70	0.64302
n-Hexadecane	C_{16}	1.3907	118.5254	0.331653	2.50	3.80078	723.000	14.00	0.71740
n-Eicosane	C_{20}	1.4340	161.8092	0.423406	2.55	4.37620	768.000	11.60	0.90688
n-Docosane	C_{22}	1.4640	185.3919	0.477206	2.49	4.58851	787.000	10.60	0.97219
n-Tetracosane	C_{24}	1.4885	208.3471	0.531299	2.40	4.90224	804.000	9.800	1.07102
n-Octacosane	C_{28}	1.5575	254.4137	0.645617	2.18	5.43355	832.000	8.500	1.23752
n-Triacontane	C_{30}	1.5811	275.6612	0.706264	2.00	5.67774	844.000	8.000	1.30718
n-Hexatriacontane	C_{36}	1.6424	342.6040	0.881442	1.70	6.34063	874.000	6.800	1.52596

The Peng–Robinson EOS was implemented in the original and traditional way, i.e., the a_c and b parameters for each fluid were calculated from T_c and P_c, while the constant m for the temperature dependence of a was calculated from the acentric factor.

3.2. Mixing rules and temperature dependence

We adopted the hypothesis that quadratic mixing rules with classic van der Waals combining rules and both an attractive and a repulsive interaction parameter should be appropriate to describe the behavior of both the methane and ethane + *n*-alkane binary systems, probably with temperature dependence for the attractive one. Indeed, we found that such dependence was required for a better capture of the phase behavior in these systems and therefore to decrease the minimum values of the objective function that could be achieved. In accordance with previous works, we implemented the following temperature dependence for both the PR and RKPR equations:

$$k_{ij} = k_{ij}^0 e^{(T/T_{c1})} \quad (1)$$

where T_{c1} is the critical temperature of the more volatile component, i.e., methane or ethane in this work. Eq. (1) can be seen as a restricted version of the functionality implemented by Cismondi et al. [5,6], where $k^\infty = 0$ (and consequently k' is now called k^0) and T^* is fixed at T_{c1}.

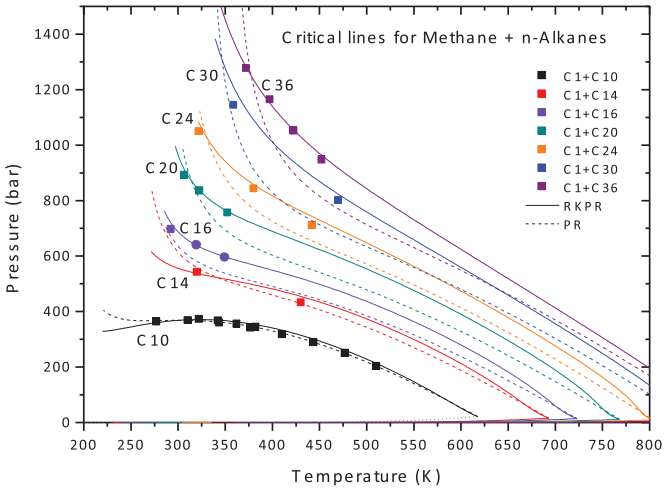

Fig. 2. Critical lines for some asymmetric methane + *n*-alkane binary systems. Calculations with the PR and RKPR EOS correspond to quadratic mixing rules with parameters from Table 3. References for the experimental critical or pseudo-critical points in Table A1.

Table 2
Type and number of experimental points (and covered *T*–*P* ranges) considered for the optimization of interaction parameters for methane and ethane + *n*-alkane systems, with the PR and RKPR EOS.

System	Critical	*x*–*y* (*T*, *P*)	Psat (*T*, *z*)	*T* range (K)	*P* range (bar)
$C_1 + C_2$	2	5	0	210.0–270.0	16.1–66.5
$C_1 + C_3$	2	8	7	144.3–360.9	2.1–94.4
$C_1 + C_4$	2	4	4	222.1–410.9	6.9–126.2
$C_1 + C_6$	2	6	3	182.5–423.0	27.6–201.6
$C_1 + C_{10}$	2	3	5	277.6–583.1	30.5–361.3
$C_1 + C_{14}$	2	0	8	294.0–540.0	20.7–464.8
$C_1 + C_{16}$	2	0	8	292.7–361.4	45.3–695.5
$C_1 + C_{20}$	2	2	6	307.4–573.2	20.1–890.0
$C_1 + C_{24}$	2	0	8	322.6–453.2	119.2–1047.0
$C_1 + C_{30}$	2	0	8	341.2–472.5	66.0–1142.0
$C_1 + C_{36}$	2	3	9	373.0–573.0	20.0–1274.0
$C_2 + C_3$	2	5	4	310.9–355.4	20.7–51.9
$C_2 + C_4$	2	7	4	303.2–394.3	17.3–58.1
$C_2 + C_5$	2	6	4	277.6–444.3	10.3–68.3
$C_2 + C_{10}$	2	6	3	277.6–510.9	6.9–118.3
$C_2 + C_{16}$	2	0	7	302.7–453.0	24.9–138.0
$C_2 + C_{20}$	2	0	8	297.2–451.5	16.5–160.5
$C_2 + C_{22}$	0	0	11	300.0–360.0	13.5–92.8
$C_2 + C_{24}$	2	0	7	302.3–360.0	11.5–144.0
$C_2 + C_{28}$	2	1	6	330.0–423.2	17.6–164.8
$C_2 + C_{36}$	2	0	6	350.0–573.2	13.6–224.0

Table 3
Optimized interaction parameters (see Eq. (1) for k_{ij}^0) and the corresponding minimum values for the objective function, for methane + *n*-alkane and ethane + *n*-alkane systems, with the PR and RKPR EOS.

System	PR EOS			RKPR EOS		
	k_{ij}^0	l_{ij}	O.F.min	k_{ij}^0	l_{ij}	O.F.min
$C_1 + C_2$	0.01122	−0.00214	0.479	0.00895	−0.00485	0.559
$C_1 + C_3$	0.03598	0.00799	1.739	0.05720	−0.00272	1.755
$C_1 + C_4$	0.09484	−0.04151	3.521	0.09984	−0.06525	3.337
$C_1 + C_6$	0.03754	−0.02993	4.848	0.01248	−0.06680	5.577
$C_1 + C_{10}$	0.13835	−0.01076	2.653	0.06891	−0.09227	4.316
$C_1 + C_{14}$	0.27424	−0.00246	8.823	0.12646	−0.11446	8.196
$C_1 + C_{16}$	0.22471	−0.02043	40.922	0.14031	−0.12441	5.511
$C_1 + C_{20}$	0.28146	−0.01030	51.873	0.11197	−0.11943	6.269
$C_1 + C_{24}$	0.31666	0.02946	87.097	0.11469	−0.09363	7.025
$C_1 + C_{30}$	0.35321	0.00845	65.713	0.12712	−0.05282	6.956
$C_1 + C_{36}$	0.41036	0.02878	70.220	0.11046	−0.02533	12.902
$C_2 + C_3$	0.04004	0.02232	0.409	0.01791	0.01332	0.582
$C_2 + C_4$	0.04618	0.00232	0.950	0.02108	−0.01748	0.917
$C_2 + C_5$	0.06878	0.01796	1.395	0.05960	−0.00102	1.459
$C_2 + C_{10}$	0.04385	0.00472	1.723	0.03023	−0.04909	1.715
$C_2 + C_{16}$	0.06611	0.00785	2.269	0.05641	−0.09261	3.382
$C_2 + C_{20}$	0.05522	0.03465	3.792	0.01552	−0.09459	3.517
$C_2 + C_{22}$	0.08321	0.02760	0.073	0.04644	−0.07507	0.091
$C_2 + C_{24}$	0.07103	0.03550	2.529	0.01398	−0.07093	4.981
$C_2 + C_{28}$	0.09670	0.04320	1.264	0.01294	−0.04895	5.242
$C_2 + C_{36}$	0.10857	0.05597	4.583	−0.01166	−0.00211	1.888

3.3. Experimental data selected and objective function

Following Cismondi et al. [6] the objective function used in this work has the following form:

$$OF = \sum_{i=1}^{NTP} \frac{(KP_i^{calc} - KP_i^{exp})^2}{KP_i^{exp}} + \sum_{j=1}^{Nz} \left[\left| \ln\left(\frac{z_{j,1}^{calc}}{z_{j,1}^{exp}}\right) \right| + \left| \ln\left(\frac{z_{j,2}^{calc}}{z_{j,2}^{exp}}\right) \right| \right] \quad (2)$$

where KP_i is either the temperature or the pressure coordinate of a binary phase equilibrium key point. The superscript "exp" means "experimental value" while the superscript "*calc*" means "calculated value".

In this work KP_i can be a critical pressure (P_c, see Tables A1 and A2 in Supplementary Material) at a specified temperature, a saturation pressure at given temperature and composition (Tables A5–A8), and also a critical end point temperature (Table A9). $z_{j,1}$ and $z_{j,2}$ are, respectively, the mole fractions of methane or ethane (1) and of the higher *n*-alkane (2). These mole fractions can be the following: the critical composition (Tables A1 and A2), the composition of a phase under two-phase equilibrium conditions at given temperature and pressure (Tables A3 and A4), or the composition of a liquid phase under conditions of LLV equilibrium (Table A10). NTP is the number of experimental pressure and temperature values used in the objective function. Analogously, N_z is the number of experimental mole fraction vectors used in the objective function. Note that the terms for temperature and pressure coordinates

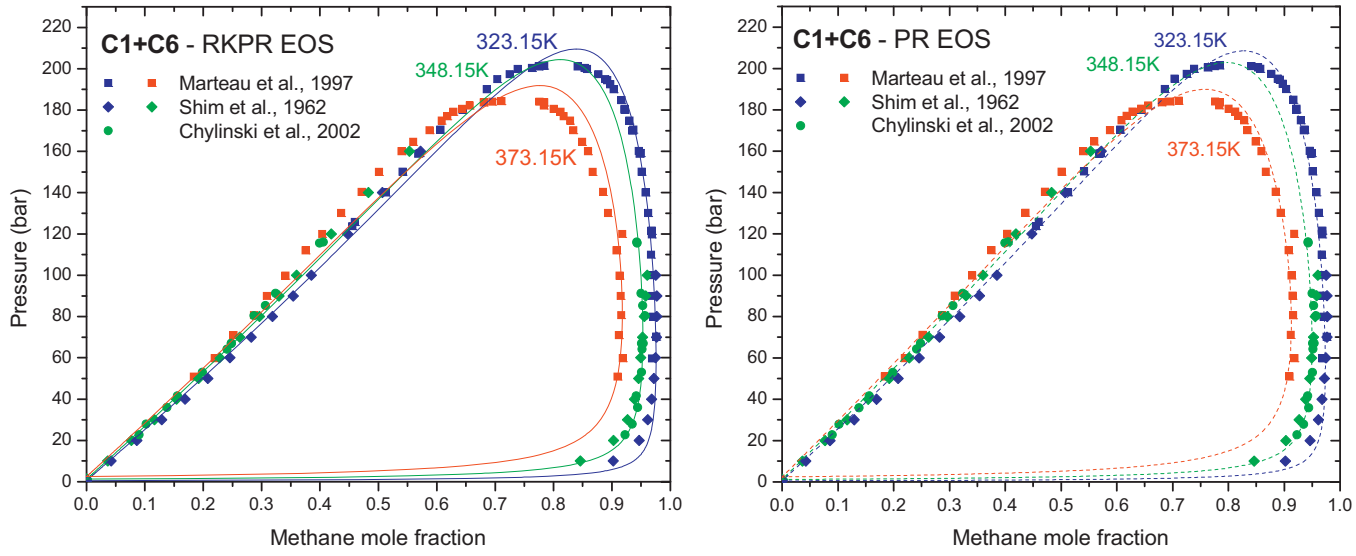

Fig. 3. Isothermal Pxy diagrams for methane + *n*-hexane at 323.15, 348.15 and 373.15 K. Calculations with the PR and RKPR EOS correspond to quadratic mixing rules with parameters from Table 3.
Source: Data taken from [28–30].

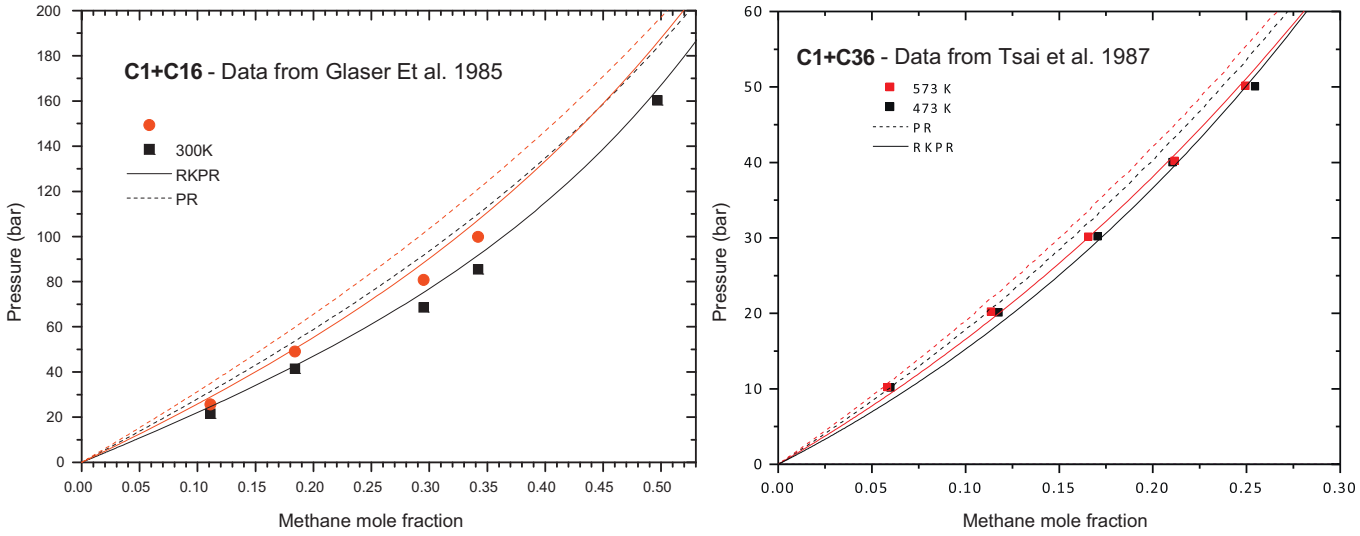

Fig. 4. Isothermal bubble pressure curves for binary mixtures of methane with *n*-hexadecane and *n*-hexatriacontane. Calculations with the PR and RKPR EOS correspond to quadratic mixing rules with parameters from Table 3.

Source: Data taken from [8,31].

are not dimensionless and that the values should be in K and bar, respectively.

Table 2 resumes the type and number of points selected for each system, together with the temperature and pressure ranges covered. The specific information and corresponding references can be found in Supplementary Material, Tables A1–A8. The number of "Psat" points for specified temperature and composition considers both bubble and dew points. For example, the number 8 indicated for the system $C_1 + C_{24}$ is the result of 6 bubble points (Table A5) plus 2 dew points (Table A7). The only type of information that is not accounted for in Table 2 is that one related to LLV behavior, since it was considered only for the systems $C_1 + C_6$ and $C_2 + C_{24}$ (Tables A9 and A10).

4. Results and discussion

Table 3 shows the optimized values for k_{ij}^0 and l_{ij}, along with the corresponding minimum value achieved for the objective function defined by Eq. (2) and Tables A1–A10 in the Supplementary Material. They are to be used with Eq. (1) for the temperature-dependence of the k_{ij} interaction parameter. For the RKPR EOS all l_{ij} values are negative (the only exception being $C_2 + C_3$), with a maximum magnitude between C_{16} and C_{20} in both series. This trend is clearly related to the trend defined for pure compound parameters in Table 1, already discussed.

4.1. The methane + n-alkane series

Fig. 2, which should be compared to Fig. 1, presents the calculated critical lines for the more asymmetric and challenging systems considered for the methane + *n*-alkane series, both with the RKPR and PR EOS. Clearly, a better agreement with experimental data is observed in general for the RKPR EOS, while PR tends to underestimate the critical pressures, at least in the systems with C_{16}, C_{20}, C_{24} and C_{30}. So this can explain part of the difference in the

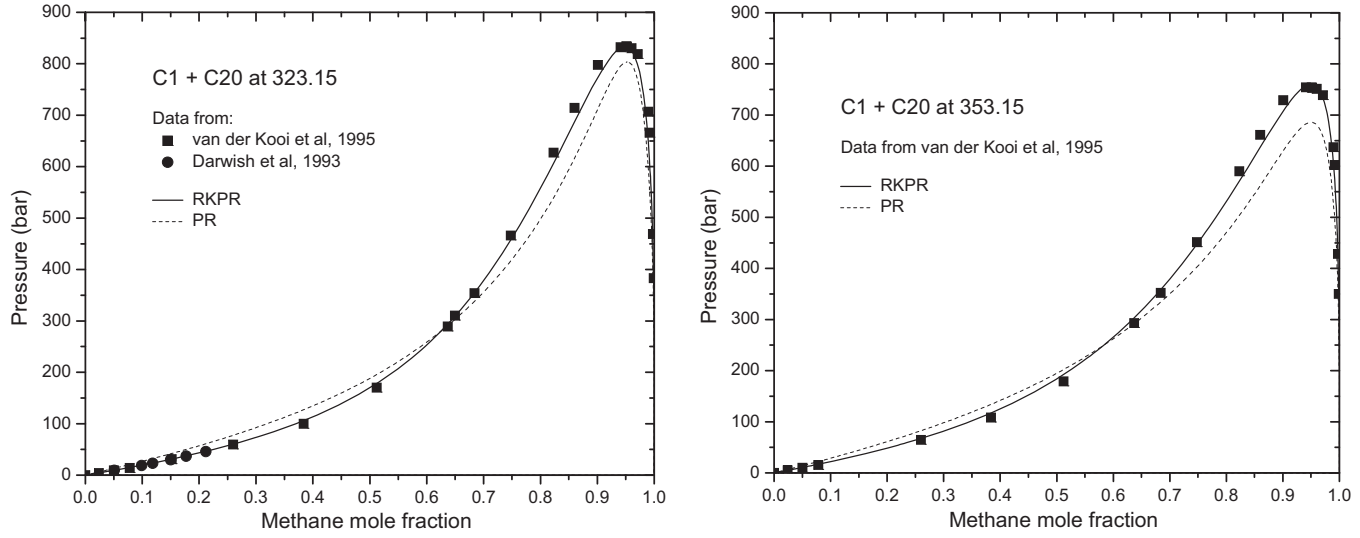

Fig. 5. Isothermal Pxy diagrams for methane + *n*-eicosane at 323.15 and 353.15 K. Calculations with the PR and RKPR EOS correspond to quadratic mixing rules with parameters from Table 3.

Source: Data taken from [12,32].

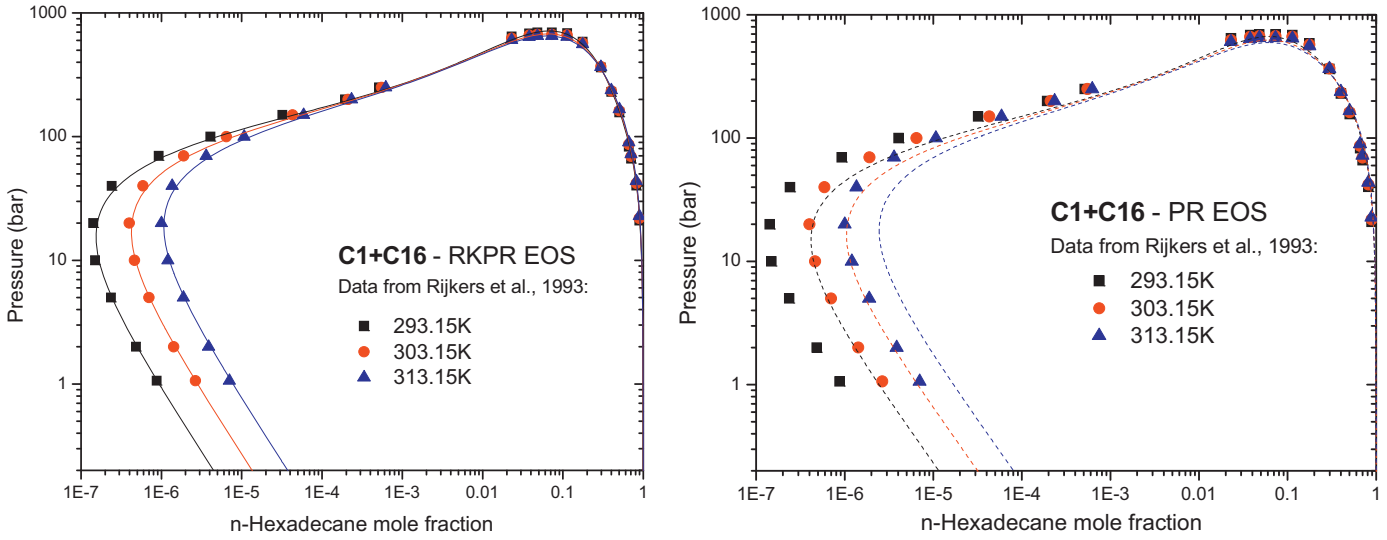

Fig. 6. Isothermal Pxy diagrams for methane + *n*-hexadecane at 293.15, 303.15 and 313.15 K. Calculations with the PR and RKPR EOS correspond to quadratic mixing rules with parameters from Table 3.

Source: Data taken from [11].

minimum values reached for the OF by each model, which increases with the asymmetry of the system (Table 3).

But the main reasons behind the obtained values in the objective function are not in the critical lines, but in the description of the biphasic behavior under them. The VLE behavior for systems with low asymmetry is well reproduced with both models, being difficult to find an important or systematic difference, as it is illustrated for $C_1 + C_6$ in Fig. 3. Nevertheless, when going to more asymmetric systems some systematic differences become evident. Different calculated isothermal VLE curves are presented in Figs. 4–6, and compared to experimental data. Fig. 4 is focused on bubble lines at low to moderate pressures for the systems with C_{16} and C_{36}. Figs. 5 and 6 present complete Pxy diagrams for $C_1 + C_{20}$ and $C_1 + C_{16}$, respectively, but in the latter case the scale is logarithmic both in pressure and molar fraction of C_{16}, in order to focus on the dew point or vapor branches. In all cases, a better performance of the RKPR EOS is observed systematically. Please note, from Tables A3, A5 and A7, that only one experimental point from those included in Fig. 6 (the dew point at 313.15 K and 150 bar) was considered in the objective function for the optimization of parameters.

The same can be observed when different isoplethic or constant composition sets of data are analyzed along the series. From Fig. B1 it can be seen that both models achieve a reasonable description of the behavior for $C_1 + C_{10}$, with deviations of different type and magnitude for the isopleths with methane molar fractions higher than 0.60, which are located in the higher pressure region. In turn, the examination of Figs. 7–9 and B2, which present similar plots for the systems with C_{16}, C_{20}, C_{24} and C_{30}, clearly show again a better performance of the RKPR EOS and larger deviations with PR, both in the low and high pressure regions.

Fig. 10 presents Pxy diagrams for $C_1 + C_{36}$, calculated at four different temperatures between 373 and 453 K in comparison to experimental data from Marteau et al. [23]. Once again, a better performance is observed for the RKPR EOS, especially at higher pressures and in both phases.

The comparisons presented through different diagrams in the previous figures are complemented with numerical deviations in the calculated saturation pressures with both models, presented in Table 4 for different asymmetric systems.

The results in Table 4 may also allow establishing comparisons with other regressions or modeling approaches. For example Gao et al. [24], in their implementation of a new and more complex mixing rule to the Patel–Teja EOS, considered some of the systems treated here, with $C_1 + C_{24}$ being the most asymmetric of them. In this case, they reported an AAD of 5.1% in saturation pressures with their proposed model, based on 283 data points taken from Flöter et al. [13] and covering pressures up to 203.9 bar. In turn, as it can be seen from Table 4, the deviations informed for $C_1 + C_{24}$ in this work are based on 421 data points from the same source, covering the whole range of pressure available for the system, which reaches more than 1000 bar. The corresponding AAD with RKPR is 3.55%.

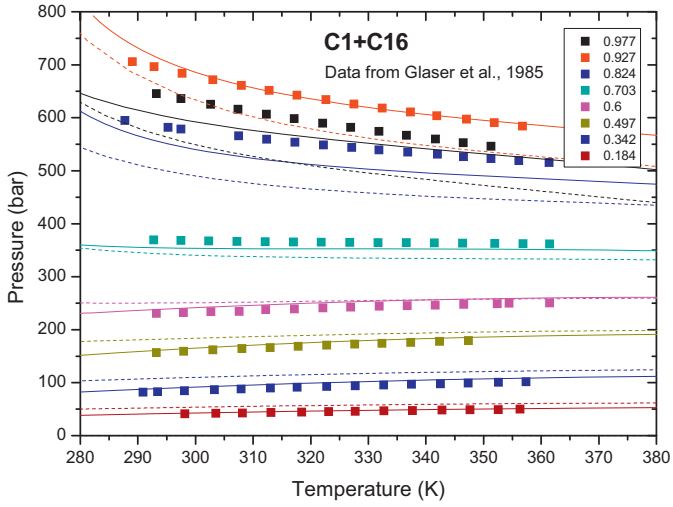

Fig. 7. Isoplethic diagrams for methane + *n*-hexadecane at different constant compositions (methane molar fractions indicated). Calculations with the PR (dashed line) and RKPR EOS (full line) correspond to quadratic mixing rules with parameters from Table 3.

Source: Data taken from [8].

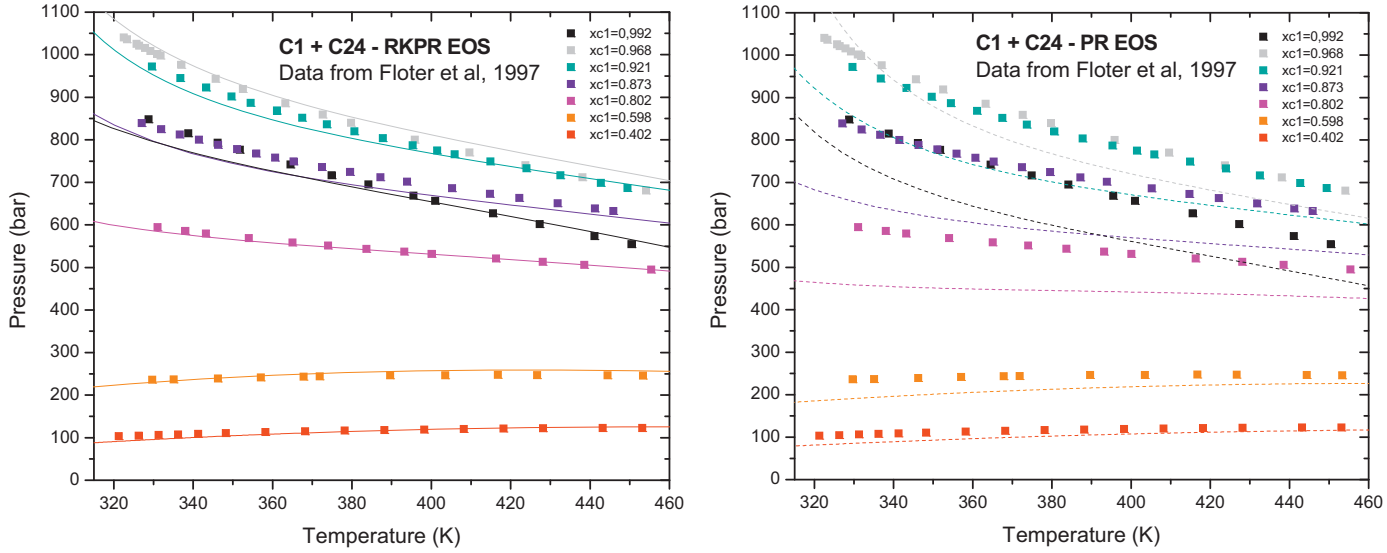

Fig. 8. Isoplethic diagrams for methane + *n*-tetracosane at different constant compositions. Calculations with the PR and RKPR EOS correspond to quadratic mixing rules with parameters from Table 3.
Source: Data taken from [13].

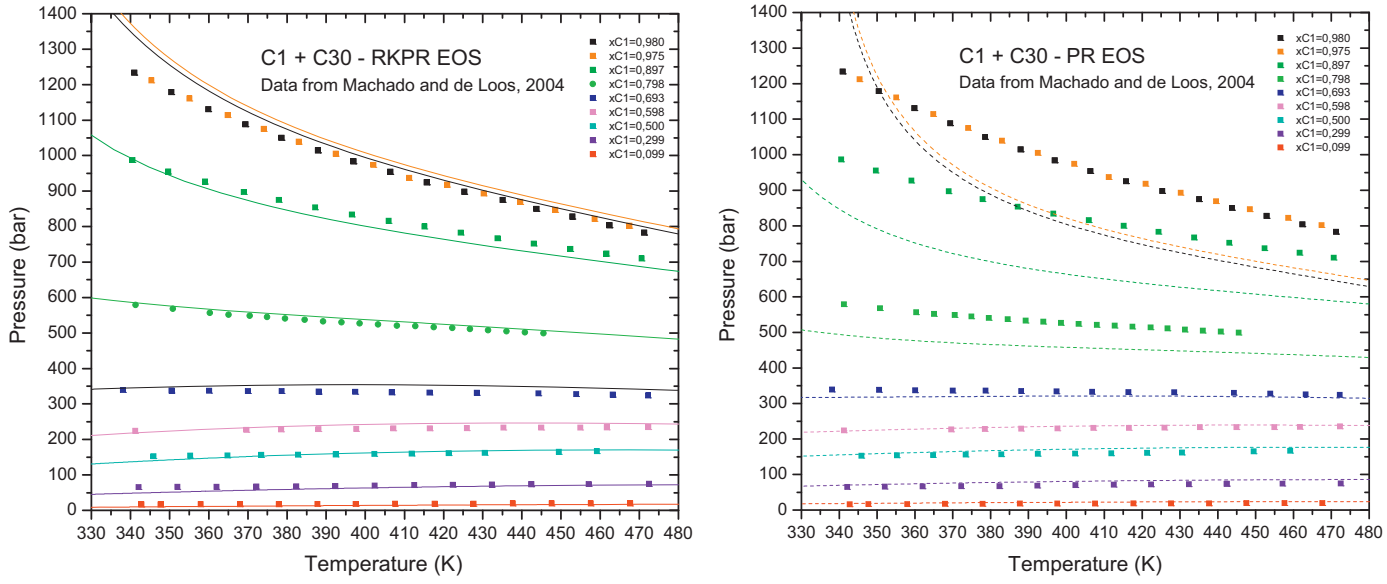

Fig. 9. Isoplethic diagrams for methane + *n*-triacontane at different constant compositions. Calculations with the PR and RKPR EOS correspond to quadratic mixing rules with parameters from Table 3.
Source: Data taken from [14].

Table 4
Comparison of percentage average absolute deviations (AAD) in saturation pressure for some methane + *n*-alkane and ethane + *n*-alkane systems, with the PR and RKPR EOS and interaction parameters from Table 3.

System	N_{iso}	*T* range (K)	*P* range (bar)	N_{data}	Reference	AAD_{PR}	AAD_{RKPR}
$C_1 + C_{20}$	20	286.5–372.3	4.0–886.7	200	Van der Kooi et al. [12]	18.25	4.98
$C_1 + C_{24}$	36	318.6–455.4	19.3–1042.6	421	Flöter et al. [13]	13.34	3.55
$C_1 + C_{30}$	10	338.1–472.5	16.4–1234.0	139	Machado and de Loos [14]	14.66	7.02
$C_2 + C_{10}$	8	307.9–353.5	32.6–86.4	32	Zamudio et al. [26]	2.59	2.15
$C_2 + C_{16}$	6	268–453.2	5.4–158.9	148	De Goede et al. [16]	3.90	6.00
$C_2 + C_{16}$	2	310–360	52.4–95.7	12	Schwarz et al. [25]	3.54	2.01
$C_2 + C_{20}$	17	292.31–451.8	2.3–168.5	174	Peters et al. [17,18]	5.99	6.45
$C_2 + C_{22}$	9	295.81–367.9	1.7–99.1	110	Peters et al. [21]	3.40	2.94
$C_2 + C_{24}$	7	136.5–368.7	4.2–129.5	76	Peters et al. [17,18]	7.83	5.61
$C_2 + C_{28}$	2	330.0–360.0	91.8–130.9	8	Schwarz et al. [25]	2.06	2.06

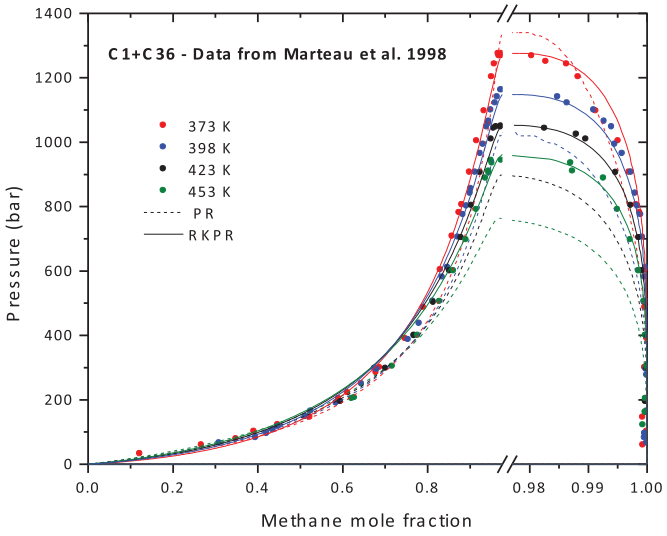

Fig. 10. Isothermal Pxy diagrams for methane + *n*-hexatriacontane at 373, 398, 423 and 453 K. Calculations with the PR and RKPR EOS correspond to quadratic mixing rules with parameters from Table 3.

Source: Data taken from [23].

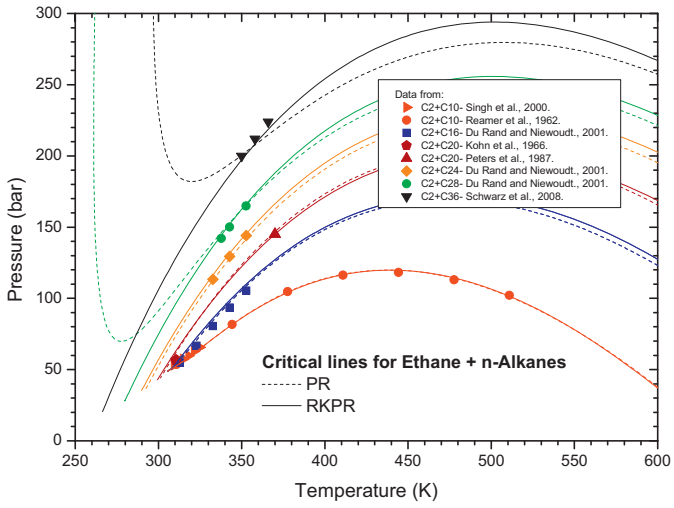

Fig. 11. Critical lines for some asymmetric ethane + *n*-alkane binary systems. Calculations with the PR and RKPR EOS correspond to quadratic mixing rules with parameters from Table 3.

4.2. The ethane + n-alkane series

In contrast to the results obtained for the methane series, where the difference in the minimum values reached for the OF increased with the asymmetry of the system and clearly favored the performance of the RKPR EOS, in this series only the system with C_{36} shows a clear difference in favor of RKPR. And the opposite is observed for the systems with C_{24} and C_{28}.

Fig. 11, which should be compared to Fig. 1, presents the calculated critical lines for the more asymmetric systems considered for the series, both with the RKPR and PR EOS. A good agreement with experimental data is observed in general for both the PR and RKPR EOS. The only important difference to note is that PR predicts phase behavior of type III for the systems with C_{28} and C_{36}. Although this could not be confirmed or discarded from experiments – due to solidification and the interruption of the critical line by a 2nd CEP [20] – the slope of the critical line calculated with RKPR agrees better with the pseudo-critical data taken from [25], leading to a phase behavior of type V (or IV) as the other less asymmetric systems.

As expected, the VLE behavior for the more symmetric systems in Table A1 is very well represented both with the PR and RKPR models. This is illustrated in Fig. 12, and also Fig. B3 in Supplementary Material, through isothermal Pxy diagrams for the systems with C_{10} and C_4, respectively. In Fig. 12 only a small underestimation of bubble pressures, which is slightly more pronounced with RKPR, is observed at the higher temperatures. In turn, RKPR describes better the composition in the vapor branches. A slightly better performance of the RKPR for $C_2 + C_{10}$ is also observed in Fig. 13, in comparison to isoplethic data in a lower temperature range. Note that these data from Zamudio et al. [26] was not considered at all in the objective function.

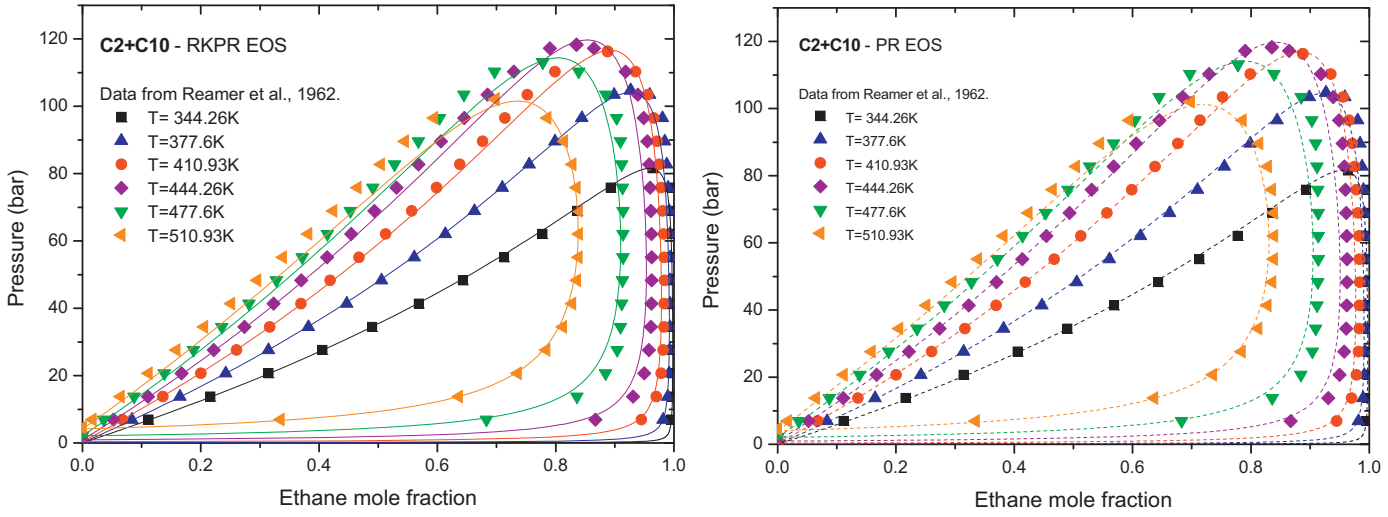

Fig. 12. Isothermal Pxy diagrams for ethane + *n*-decane at six different temperatures. Calculations with the PR and RKPR EOS correspond to quadratic mixing rules with parameters from Table 3.

Source: Data taken from [33].

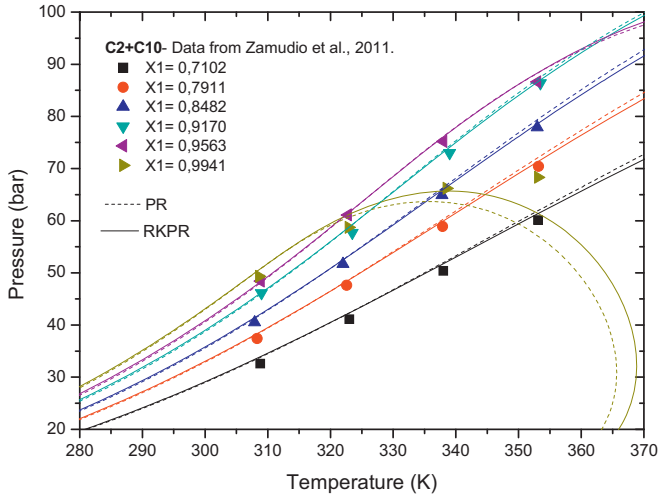

Fig. 13. Isoplethic diagrams for ethane + *n*-decane at different constant compositions (ethane molar fractions indicated). Calculations with the PR and RKPR EOS correspond to quadratic mixing rules with parameters from Table 3.
Source: Data taken from [26].

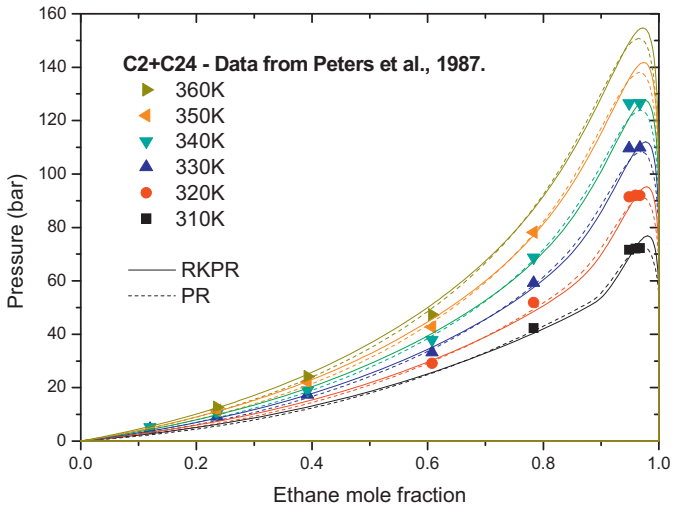

Fig. 15. Isothermal Pxy diagrams for ethane + *n*-tetracosane at six different temperatures. Calculations with the PR and RKPR EOS correspond to quadratic mixing rules with parameters from Table 3.
Source: Data taken from [22].

Quite similar and good performances of both models can be observed for the system with C_{16} through the comparison to isoplethic data in a wide range of temperature covering from 260 to almost 460 K (Fig. 14) and to Pxy data in the critical region for five temperatures from 312.9 to 352.7 K (Fig. B4). The same is valid for C_{24}, C_{20} and C_{22} through the observation of isothermal Pxy diagrams in Figs. 15, B5 and B6, respectively. A clear difference between the predictions from both models only appears in the vapor branches in a logarithmic scale for the molar fraction of C_{20} (Fig. B5), with the RKPR showing better agreement with the data at 370 K and PR at 330 K.

Fig. 16 presents isothermal bubble pressure curves for $C_2 + C_{28}$ and $C_2 + C_{36}$ at three temperatures for each system. Opposite to what was found in the study for the methane-series, here the RKPR systematically predicts slightly higher bubble pressures than the PR EOS, which is coincident with Figs. 15 and B4 for this range of compositions richer in the heavy component. But depending on both temperature and composition one or the other model can be closer to experimental data.

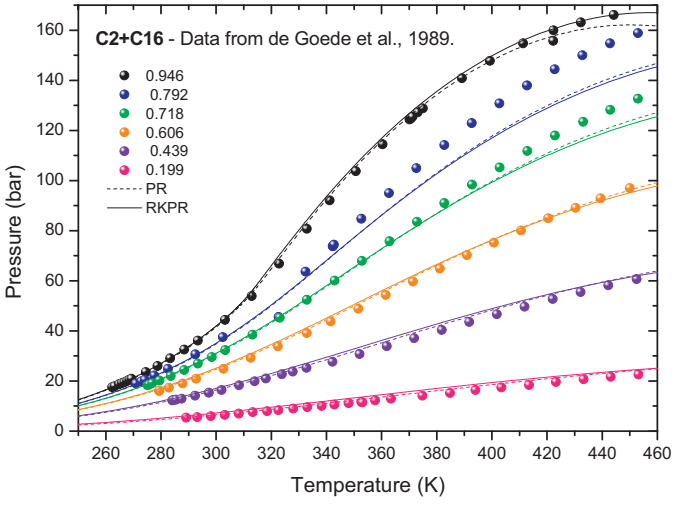

Fig. 14. Isoplethic diagrams for ethane + *n*-hexadecane at different constant compositions (ethane molar fractions indicated). Calculations with the PR and RKPR EOS correspond to quadratic mixing rules with parameters from Table 3.
Source: Data taken from [16].

Fig. 17 presents a comparison between calculated isothermal Pxy diagrams and experimental data in the high pressure and critical region for $C_2 + C_{36}$. A reasonable agreement with the experimental data on the liquid branches is observed for both models, but the vapor branches are clearly better described by the RKPR EOS.

In summary, we find that, different to the observations for the methane-series, in this case there is no clear advantage for the RKPR over the PR EOS in the description of the fluid phase behavior, except a better representation of vapor phase compositions in some systems.

A final comment is necessary regarding the possibility of extending the study to other three-parameter EOS, in particular Patel–Teja (PT) [27] which is probably the most popular one. When the original parameterization procedures proposed for both models are relaxed, the only real difference that remains between the PT and the RKPR equations is in the alpha function. The volumetric dependence of the attractive terms looks different just because of the way the third parameter is defined in each case, but they can be converted one to each other, as it is shown in Ref. [2]. In the implementation for mixtures, there could also be an effect from the linear mixing rule applied to one third parameter or the other, but such differentiation effect is expected to be negligible. In other words, the pure compound parameters for the RKPR EOS in Table 1 are expected to give very similar results with the PT EOS if the values for δ_1 are converted into the corresponding c values and the chosen alpha function is adjusted to match the acentric factor with the PT EOS. Accordingly, the interaction parameters in Table 3 are also expected to produce similar results with the PT equation (if used together with pure compound parameters equivalent to those in Table 1), but some differences might appear depending on the alpha function implemented.

5. Conclusions

A new table of RKPR pure compound parameters for *n*-alkanes from C_1 to C_{36} was defined, with the objective of promoting an

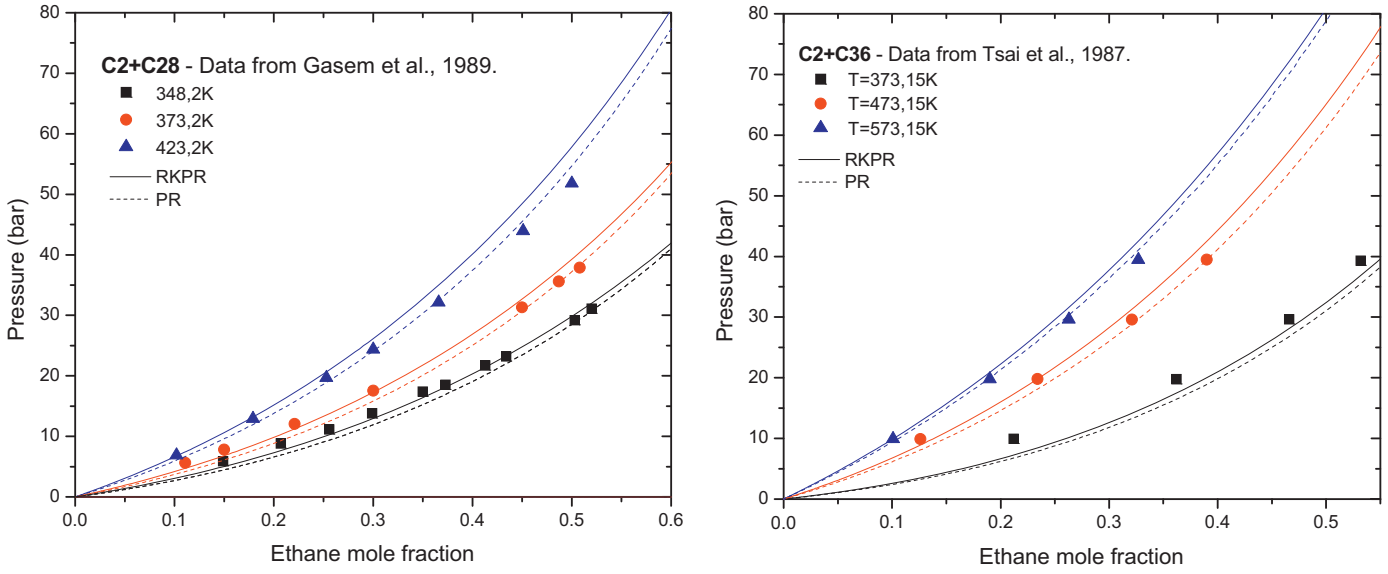

Fig. 16. Isothermal bubble pressure curves for binary mixtures of ethane with *n*-octacosane and *n*-hexatriacontane. Calculations with the PR and RKPR EOS correspond to quadratic mixing rules with parameters from Table 3.
Source: Data taken from [31,34].

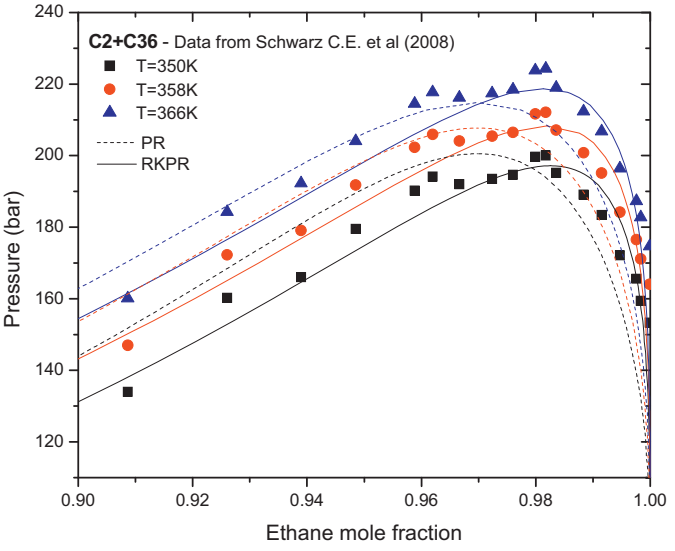

Fig. 17. High pressure sections of isothermal Pxy diagrams for ethane + *n*-hexatriacontane at 350, 358, and 366 K. Calculations with the PR and RKPR EOS correspond to quadratic mixing rules with parameters from Table 3.
Source: Data taken from [25].

improved description of the phase behavior for the asymmetric mixtures between them while observing a regular trend along the whole series.

Based on carefully designed objective functions, with selected data points covering the wider possible ranges of temperature and pressure depending on the availability of information in the literature, attractive and repulsive interaction parameters were obtained for 11 methane + *n*-alkane and for 10 ethane + *n*-alkane binary systems, for both the PR and the RKPR EOS with the new parameter table. Although the attractive interaction was made temperature-dependent, the chosen functionality always tends to zero for infinite temperature, and the reference temperature was fixed to the critical temperature of the light component in each series. Therefore only two constants were fitted per binary: k_{ij}^0 and l_{ij}.

Results clearly show a better representation of the phase behavior for the more asymmetric systems with the RKPR EOS in comparison to the Peng–Robinson EOS. That was observed in terms of critical lines, bubble pressures, solubility curves of the heavy alkane in the vapor or light phase and also in complete sets of isopleths in wide ranges of pressure. Still, the performance of the RKPR EOS for some specific systems like those of methane with C_6, C_{10} and C_{14} is not as good as one might expect from the results for the other systems. This could be related to the quality of some experimental points and a possible bad balance among the data selected for the objective function of the system.

Despite the good results achieved in terms of the fluid phase behavior of methane + *n*-alkane binary systems in the temperature–pressure-composition space, a price is expected to be paid in the description of volumetric properties, in comparison to previous implementations of the RKPR model with other sets of pure compound parameters. Nevertheless, that was never a strong point of cubic equations of state, and moreover it could be corrected through different empirical approaches.

In the case of ethane + *n*-alkane systems the results were quite good for both models and no clear difference was observed, despite some systematic trends which do not seem to imply an advantage for one or the other model when comparisons are made to experimental data. Probably, the only exception is for some systems a better prediction of the solubility of the heavy compound in the vapor phase with RKPR. The fact that an advantage of the RKPR model did not become evident for this series could be related in part to the unavailability of data at higher temperatures and pressures for the more asymmetric systems (where a higher immiscibility is expected at high pressures, see Fig. 11) and, more important, to the lower asymmetry considered here in comparison to the study for the methane-series. Based on different possible measures, like evolution in the type of phase behavior, shape and pressure level of critical lines, molecular weights, pure compound EOS parameters, etc., the asymmetry of $C_2 + C_{36}$ could be comparable to that of C_1 with carbon numbers between 10 and 16. Indeed, only in that range of carbon numbers the superiority of RKPR EOS with the new pure compound table started to become evident in the series with methane.

Finally, the regularity observed both in the interaction parameters obtained and on the predictions for the different systems, suggests developing a correlation of the binary interaction parameters for each series of binary mixtures in terms of the carbon

number of the larger compound. That could bring two benefits: first to correct or compensate for the effects of uncertainty and distribution in the data selected for each system, and second the predictive capacity that would be gained for systems with no availability of experimental data.

List of symbols

a_c	attractive parameter for each fluid in the PR or RKPR EOS
b	co-volume or repulsive parameter for each fluid in the PR or RKPR EOS
EOS	equation of state
k_{ij}	attractive interaction parameter in quadratic mixing rules
l_{ij}	repulsive interaction parameter in quadratic mixing rules
LLVE	liquid liquid vapor equilibrium
P_c	critical pressure
PR	Peng–Robinson
RKPR	generalized Redlich–Kwong–Peng–Robinson EOS
SRK	Soave Redlich–Kwong
T_c	critical temperature
T_r	relative temperature
VLE	vapor liquid equilibrium
Z_c^{EOS}	critical compressibility factor predicted from an EOS
Z_c^{EXP}	experimental critical compressibility factor
δ_1	third parameter in the RKPR EOS
ω	acentric factor

Acknowledgments

We acknowledge the financial support received from the following Argentinean institutions: Consejo Nacional de Investigaciones Científicas y Técnicas de la República Argentina, Agencia Nacional de Promoción Científica y Tecnológica de la República Argentina and Universidad Nacional de Córdoba.

Appendix A. Supplementary data

Supplementary data associated with this article can be found, in the online version, at http://dx.doi.org/10.1016/j.fluid.2013.09.039.

References

[1] K.S. Pedersen, P.L. Christensen, Phase Behavior of Petroleum Reservoir Fluids, CRC/Taylor & Francis, 2006.
[2] M. Cismondi, J. Mollerup, Development and application of a three-parameter RK-PR equation of state, Fluid Phase Equilibria 232 (2005) 74–89.
[3] S.A. Martinez, K.R. Hall, Thermodynamic properties of light synthetic natural gas mixtures using the RK-PR cubic equation of state, Industrial and Engineering Chemistry Research 45 (2006) 3684–3692.
[4] A.R.J. Arendsen, G.F. Versteeg, Dynamic thermodynamics with internal energy, volume, and amount of moles as states: application to liquefied gas tank, Industrial and Engineering Chemistry Research 48 (2009) 3167–3176.
[5] M. Cismondi, J.M. Mollerup, M.S. Zabaloy, Equation of state modeling of the phase equilibria of asymmetric CO_2 + *n*-alkane binary systems using mixing rules cubic with respect to mole fraction, Journal of Supercritical Fluids 55 (2010) 671–681.
[6] M. Cismondi, S.B. Rodríguez-Reartes, J.M. Milanesio, M.S. Zabaloy, Phase equilibria of CO_2 + *n*-alkane binary systems in wide ranges of conditions: development of predictive correlations based on cubic mixing rules, Industrial & Engineering Chemistry Research 51 (2012) 6232–6250.
[7] S.K. Kim, H.S. Choi, Y. Kim, Thermodynamic modeling based on a generalized cubic equation of state for kerosene/LOx rocket combustion, Combustion and Flame 159 (2012) 1351–1365.
[8] M. Glaser, C.J. Peters, H.J. Van Der Kool, R.N. Lichtenthaler, Phase equilibria of (methane + *n*-hexadecane) and (p, Vm, T) of *n*-hexadecane, Journal of Chemical Thermodynamics 17 (1985) 803–815.
[9] V.V. de Leeuw, T.W. de Loos, H.A. Kooijman, J. de Swaan Arons, The experimental determination and modelling of VLE for binary subsystems of the quaternary system $N_2 + CH_4 + C_4H_{10} + C_{14}H_{30}$ up to 1000 bar and 440 K, Fluid Phase Equilibria 73 (1992) 285–321.
[10] M.P.W.M. Rijkers, M. Malais, C.J. Peters, J. de Swaan Arons, Measurements on the phase behavior of binary hydrocarbon mixtures for modelling the condensation behavior of natural gas. Part I. The system methane + decane, Fluid Phase Equilibria 71 (1992) 143–168.
[11] M.P.W.M. Rijkers, C.J. Peters, J. de Swaan Arons, Measurements on the phase behavior of binary mixtures for modeling the condensation behavior of natural gas. Part III. The system methane + hexadecane, Fluid Phase Equilibria 85 (1993) 335–345.
[12] H.J. van der Kooi, E. Flöter, T.W.d. Loos, High-pressure phase equilibria of $\{(1-x)CH_4 + xCH_3(CH_2)18CH_3\}$, Journal of Chemical Thermodynamics 27 (1995) 847–861.
[13] E. Flöter, T.W. De Loos, J. De Swaan Arons, High pressure solid-fluid and vapour–liquid equilibria in the system (methane + tetracosane), Fluid Phase Equilibria 127 (1997) 129–146.
[14] J.J.B. Machado, T.W. De Loos, Liquid–vapour and solid-fluid equilibria for the system methane + triacontane at high temperature and high pressure, Fluid Phase Equilibria 222–223 (2004) 261–267.
[15] E. Flöter, T.W. de Loos, J. de Swaan Arons, Hyperbaric reservoir fluids: high-pressure phase behavior of asymmetric methane + *n*-alkane systems, International Journal of Thermophysics 16 (1995) 185–194.
[16] R. De Goede, C.J. Peters, H.J. Van Der Kooi, R.N. Lichtenthaler, Phase equilibria in binary mixtures of ethane and hexadecane, Fluid Phase Equilibria 50 (1989) 305–314.
[17] C.J. Peters, J.L. De Roo, J. De Swaan Arons, Three-phase equilibria in (ethane + pentacosane), Journal of Chemical Thermodynamics 19 (1987) 265–272.
[18] C.J. Peters, J.L. De Roo, R.N. Lichtenthaler, Measurements and calculations of phase equilibria of binary mixtures of ethane + eicosane. Part I: vapour + liquid equilibria, Fluid Phase Equilibria 34 (1987) 287–308.
[19] C.J. Peters, J.L. de Roo, R.N. Lichtenthaler, Measurements and calculations of phase equilibria in binary mixtures of ethane + eicosane. Part 3. Three-phase equilibria, Fluid Phase Equilibria 69 (1991) 51–66.
[20] C.J. Peters, R.N. Lichtenthaler, J. de Swaan Arons, Three phase equilibria in binary mixtures of ethane and higher *n*-alkanes, Fluid Phase Equilibria 29 (1986) 495–504.
[21] C.J. Peters, J. Spiegelaar, J. De Swaan Arons, Phase equilibria in binary mixtures of ethane + docosane and molar volumes of liquid docosane, Fluid Phase Equilibria 41 (1988) 245–256.
[22] C.J. Peters, H.J. Van Der Kooi, J. De Swaan Arons, Measurements and calculations of phase equilibria for (ethane + tetracosane) and (p, Vm′ *, T) of liquid tetracosane, Journal of Chemical Thermodynamics 19 (1987) 395–405.
[23] P. Marteau, P. Tobaly, V. Ruffier-Meray, J.C. De Hemptinne, High-pressure phase diagrams of methane + squalane and methane + hexatriacontane mixtures, Journal of Chemical and Engineering Data 43 (1998) 362–366.
[24] J. Gao, L.D. Li, Z.Y. Zhu, S.G. Ru, Vapor–liquid equilibria calculation for asymmetric systems using Patel–Teja equation of state with a new mixing rule, Fluid Phase Equilibria 224 (2004) 213–219.
[25] C.E. Schwarz, I. Nieuwoudt, J.H. Knoetze, Phase equilibria of long chain *n*-alkanes in supercritical ethane: review, measurements and prediction, Journal of Supercritical Fluids 46 (2008) 226–232.
[26] M. Zamudio, C.E. Schwarz, J.H. Knoetze, Phase equilibria of branched isomers of C_{10}-alcohols and C_{10}-alkanes in supercritical ethane, Journal of Supercritical Fluids 58 (2011) 330–342.
[27] N.C. Patel, A.S. Teja, A new cubic equation of state for fluids and fluid mixtures, Chemical Engineering Science 37 (1982) 463–473.
[28] J. Shim, J.P. Kohn, Multiphase and volumetric equilibria of methane-*n*-hexane binary system at temperatures between −110 °C and 150 °C, Journal of Chemical and Engineering Data 7 (1962) 3–8.
[29] P. Marteau, J. Obriot, A. Barreau, V. Ruffier-Meray, E. Behar, Experimental determination of the phase behavior of binary mixtures: methane–hexane and methane–benzene, Fluid Phase Equilibria 129 (1997) 285–305.
[30] K. Chylinski, M.J. Cebola, A. Meredith, G. Saville, W.A. Wakeham, Apparatus for phase equilibrium measurements at high temperatures and pressures, Journal of Chemical Thermodynamics 34 (2002) 1703–1728.
[31] F.N. Tsai, S.H. Huang, H.M. Lin, K.C. Chao, Solubility of methane, ethane, and carbon dioxide in *n*-hexatriacontane, Journal of Chemical and Engineering Data 32 (1987) 467–469.
[32] N.A. Darwish, J. Fathikalajahi, K.A.M. Gasem, R.L. Robinson Jr., Solubility of methane in heavy normal paraffins at temperatures from 323 to 423 K and pressures to 10.7 MPa, Journal of Chemical and Engineering Data 38 (1993) 44–48.
[33] H.H. Reamer, B.H. Sage, Phase equilibria in hydrocarbon systems: volumetric and phase behavior of the ethane-*n*-decane system, Journal of Chemical and Engineering Data 7 (1962) 161–168.
[34] K.A.M. Gasem, B.A. Bufkin, A.M. Raff, R.L. Robinson, Solubilities of ethane in heavy normal paraffins at pressures to 7.8 MPa and temperatures from 348 to 423 K, Journal of Chemical and Engineering Data 34 (1989) 187–191.